Research Article / Araştırma Makalesi

CALIBRATION OF CHABOCHE KINEMATIC HARDENING MODEL PARAMETERS BY OPTIMISATION

CHABOCHE KİNEMATİK PEKLEŞME MODELİ PARAMETRELERİNİN OPTİMİZASYON İLE KALİBRE EDİLMESİ

Alişan ARASLI[1]   **İlyas KACAR[2]**

Abstract

Drag links are used in the automotive industry mostly, and during painting, their ends are protected against paint by two types of cap productions. While one is machined, the other is cold formed. In this study, a finite element simulation for the deformation process of a drag link's cap made from St52 alloy is performed. For the plasticity model, Chaboche's nonlinear kinematic hardening rule is used with the associated flow rule and Von Mises yield criterion. Chaboche's parameters are determined by low cycle fatigue test by applying curve fitting methods to one hysteresis loop. Furthermore, the Chaboche model parameters are calibrated by the optimization process. The final diameters of the cap measurements are compared with those obtained from the optimized model. Therefore, a comprehensive methodology is presented for the determination and calibration of Chaboche kinematic hardening model parameters. Chaboches calibrated parameters are YS=370,73 MPa, C=3513,5 MPa, and γ=47,958 while their initial values are YS=360 MPa, C=3500 MPa, and γ=90.

Keywords: Chaboche model, kinematic hardening, optimization, low cycle fatigue, Cold forming, plasticity.

Öz

Rot kolu çoğunlukla otomotiv endüstrisinde kullanılmakta ve boyama sırasında uçları iki tip kapak üretim yöntemiyle boyaya karşı korunmaktadır. Bunlardan biri talaşlı imalat, diğeri ise soğuk şekillendirmedir. Bu çalışmada, St52 alaşımından yapılmış bir rot kolunun kapağının deformasyon işlemi için bir sonlu elemanlar simülasyonu gerçekleştirilmiştir. Plastisite modelini oluşturmak için Chaboche'nin doğrusal olmayan kinematik pekleşme kuralı, ilişkili akış kuralı ve Von Mises akma kriteri kullanılmıştır. Chaboche parametreleri, bir histerezis döngüsüne eğri uydurma yöntemleri uygulanarak düşük çevrimli yorulma testi ile belirlenmiştir. Ayrıca, Chaboche model parametreleri optimizasyon işlemi ile kalibre edilmiştir. Kapak ölçümlerinin nihai çapları, optimize edilmiş modelden elde edilenlerle karşılaştırılmıştır. Chaboche kinematik pekleşme modelinin parametrelerinin belirlenmesi ve kalibrasyonu için kapsamlı bir yöntem sunulmuştur. Kalibre edilen Chaboche parametreleri YS=370,73 MPa, C=3513,5 MPa ve γ=47,958 iken başlangıç değerleri YS=360 MPa, C=3500 MPa ve γ=90'dır.

Anahtar Kelimeler: Chaboche modeli, kinematik pekleşme, optimizasyon, düşük çevrimli yorulma, soğuk şekillendirme, plastisite.

[1] Şeyh Şamil., Ankara, Türkiye.
 alisanarasli@gmail.com, Orcid.org/0000-0002-3724-5429.

[2] Niğde Ömer Halisdemir University, Engineering Faculty, Department of Mechatronics Engineering, Niğde, Türkiye.
 ikacar@gmail.com, Orcid.org/0000-0002-5887-8807.

1. INTRODUCTION

Drag links are used to change the direction of the vehicle by transferring the steering movement to the wheels in heavy and light commercial vehicles (Ditas, 2019). The drag link consists of 33 critical parts, including two rod ends. One of the most critical parts of a drag link is the ball joint. An example of the drag link and details of the rod end are shown in Figure 1.

(*a*) The assembly of the drag link   (*b*) Details of the rod end
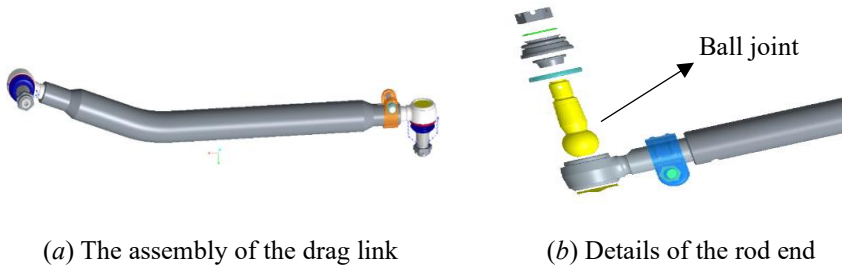
Figure 1. Drag Link

Drag links are mounted on the vehicle with the help of a ball joint and nut. Fixing of the drag link to the vehicle is shown in Figure 2.
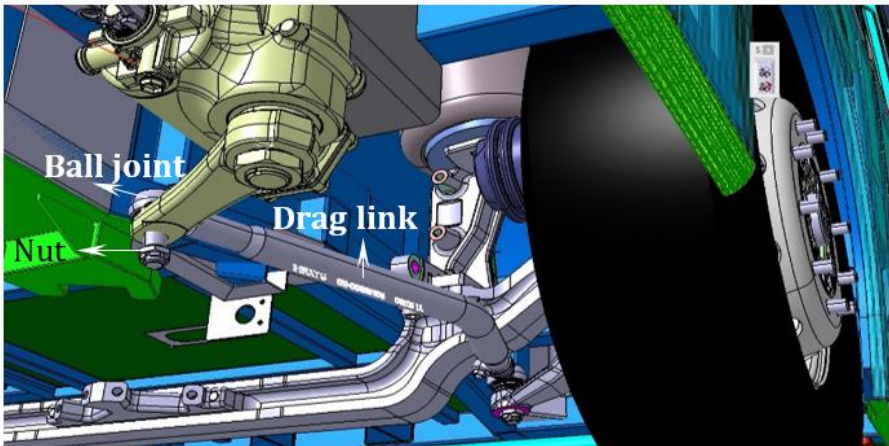
Figure 2. Drag Link Assembly on The Vehicle

As shown in Figure 2, the ball joint and nut are of high importance during assembly. Therefore, any faults in the ball joint and nut threads will become a problem during the assembly phase. In this regard, the most common fails are seen in the machining and painting process. Fails in the painting process are shown in Figure 3-*a*.

Figure 3. Process Faults and Cleaning Brush
(*a*) A Fail in The Painting Process (*b*) Cleaning Brush

Because of this fail, the ball joint threads must be cleaned with an additional brushing operation to ensure well-suit between the joint and the nut. The cleaning brush is shown in Figure 3-*b*. Kaizen studies were conducted in Ditaş Corp. to prevent these fails in the painting operation (Ditaş, 2019). It was decided to make paint protection caps based on the results of these Saizen studies. Paint protection caps are shown in Figure 4.
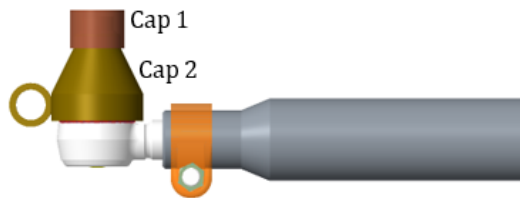
Figure 4. Paint Protection Caps

The cap 1 is produced during the machining operation. It is for clamping the end of the ball joint. Thus, it allows connection with cap 2. The cap 2 is produced in the cold forming process. Any small defect seen in the paint process affects the vehicle assembly. Thus, the cold-forming process must be performed accurately. Therefore, accurate mold dimensions and forming force are required for accurate results. Finite element simulations are an effective tool for predicting process parameters by simulating deformation processes (Kacar, 2023). Plasticity theories are used to determine the amount of plastic deformation (ε^p) in a deformation process. However, the determination of the plastic part of the deformation requires a flow criterion, a hardening rule, and a flow rule. There are 2 types of hardening rules in the simulations. These are the isotropic and the kinematic rule. Combining of both is possible. In this study, Chaboche's hardening model, which is a type of kinematic hardening model, was used.

First, with Prager's hardening rule (Prager, 1949), linear kinematic hardening was included in simulations and then modified by (Ziegler, 1959). However, these linear hardening plasticity models are not sufficient to predict the Bauschinger effect, multiaxial ratcheting, plastic strain accumulation, or shakedown. Therefore, nonlinear

kinematic models were developed on the basis of the equation of Armstrong and Frederick (Armstrong and Frederick, 1966). Armstrong and Frederick's rule includes a strain hardening and recovery term in their equation. Then, based on changing the dynamic-recovery term in the formula of Armstrong and Frederick, many other hardening plasticity models were developed, one of which was Chaboche's plasticity model (Chaboche, 1986; Chaboche, 1989, Cruise & Gardner, 2008).

In industry, there are many applications of cold forming processes performed on many materials. In addition, cold forming is used in most materials, including stainless steel [8] and two grades of carbon steel (Kuhn et al., 1973). However, there is no study on the 70x3-mm pipe made from St52 alloy which is cold-formed for the paint protection caps. It has axially symmetrical geometry (Sevenler et al., 1987).

The aim of this study is to determine the best hardening model parameters for the production of the protection caps made by cold deformation. It is a process in which plastic flow occurs due to both contact and large deformation. In order to simulate this process with high accuracy, a constitutive model should be used in the simulation. A constitutive model includes 3 aspects: Yield criterion, hardening rule, and flow rule. However, the selection of the constitutive equation model and its parameters is a big problem. Because many issues require fine tuning the model parameters such as different material, different deformation process, different geometry, different temperature, different deformation rate, etc.. This fine tuning process is called calibration. In this study, the constitutive equation is established and the hardening rule is calibrated to be used for cap deformation.

In this study, the Chaboche's nonlinear kinematic hardening parameters for 70x3-mm St52 steel pipe are determined by applying curve fitting methods to the tension–compression cycling test data. These data are used to constitute a plasticity model for simulation based on finite element method. The deformation has cold forming process of the painting protection cap on the drag link. Furthermore, the Chaboche model parameters were calibrated by an optimization process. Finally, the directional deformations measured experimentally are compared with those obtained from the optimized model. Therefore, a comprehensive methodology is presented for the determination and calibration of Chaboche kinematic hardening model parameters.

2. COLD FORMING

Plastic deformation of the work piece with a load applied without the need for temperature is called cold forming. The heating phase applied in hot forming processes is not present in cold forming. Because of the friction force during deformation, a slight increase in temperature can be observed in the work piece. In addition, cold forming processes in small diameters are preferred because they are faster than hot forming. Figure 5 shows the setup of the cold forming process. Figure 5-*a* shows the location of the punch, pipe, and die. Figure 5-*b* shows their details.
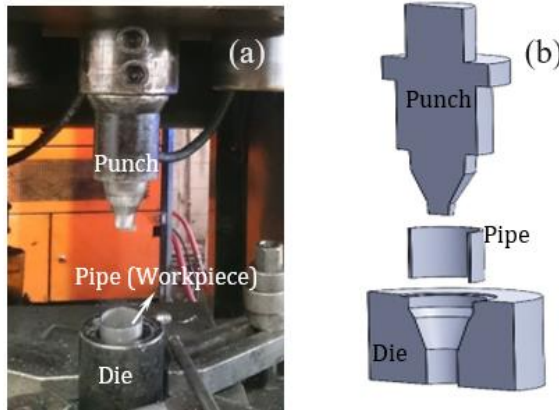
Figure 5. Set-up of The Cold Forming Process
(*a*) Mold and Work Piece (*b*) Cutaway View

In general, cold forming is performed on a work piece placed on a fixed bottom mold by the load application of the movable upper punch. While one end contracts, the other end's diameter does not change. However, between both ends, large deformation occurs. In the finite element simulation, we must create frictional contacts between the pipe and the mold surface. To provide permanent deformation on the cap (deformed pipe), the analysis must include a plasticity model. Frictional contact, large deflection, and plastic deformation lead the analysis to nonlinear behaviour inherently.

3. MATERIAL AND METHOD

As material, St52 alloy is used. Its elemental composition is given in Table 1.

Table 1. Chemical Composition (weight %) of The St52 Alloy

C	Si	Mn	P	S	Cr	Ni	Mo
0,19	0,406	1,37	0,018	0,0072	0,04	0,08	0,015
Al	Cu %	Co	Ti	Nb	V	W	Pb
0,047	0,04	0,005	<0,0010	<0,0030	<0,0010	0,025	<0,0030
B	Sn	Zn	As	Bi	Ca	Ce	Fe
<0,0005	0,0085	0,0044	0,008	<0,0020	0,0005	<0,0030	<97,7

The hardening model parameters' determining and calibration is given in Figure 6 schematically. It describes the plasticity model.
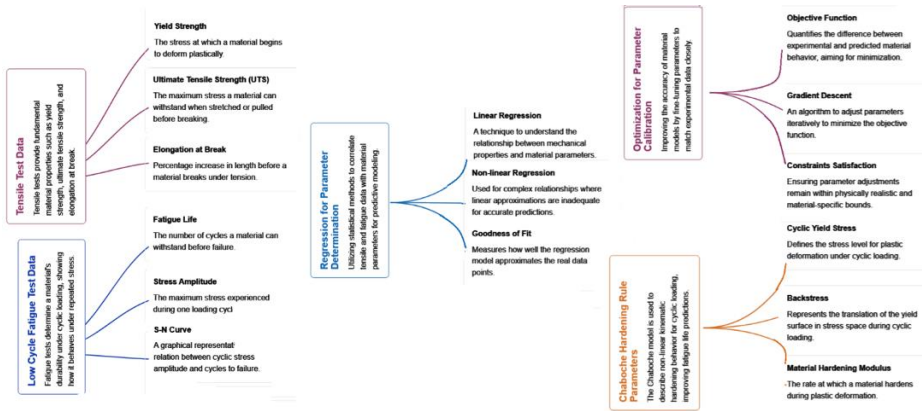
Figure 6. Schematic Representation of The Calibration of A Plasticity Model

3.1. Monotonic Tensile Test

A tensile test bench was used to determine the mechanical properties of the St52 alloy. Rectangular dog-bone-shaped specimens are prepared following the ASTM E8 standard [25]. The dimensions of the specimen are shown in Figure 7-*a*. Tensile tests were performed on a Shimadzu Autograph 100 kN testing machine with a data acquisition system maintained by a digital interface board using a specialized computer program. Material deformation is measured using a video-type extensometer measurement system. The tensile tests are performed at 25 mm/min (0,0083 Hz for a 50-mm gage length) strain rate. The test is performed at room temperature. The result of monotonic tensile test is shown in Figure 7-*b*. The diagram includes the true stress and true total strain.
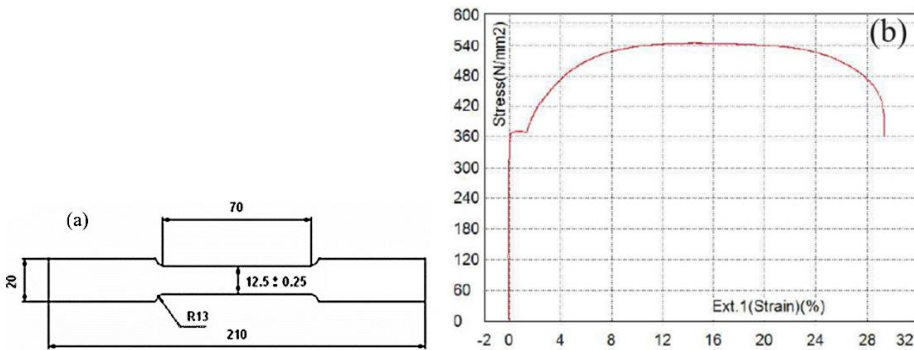
Figure 7. (*a*) Specimen Dimensions For Monotonic Tensile Test (in mm)
(*B*) Test Data

Table 2. Mechanical Properties of St52 Steel

Property	Value
Density (gr/cm³)	7,85
Young modules 8GPa)	207
Poisson ratio	0,28
Yield strength (MPa)	373,806
Ultimate tensile strength (MPa)	414,047

3.2. Low Cycle Fatigue Test

Low cycle fatigue (LCF) tests give curves called hysteresis loops. Since these curves exhibit the material's hardening, they are also used to determine the hardening model parameters. In fact, one loop is sufficient to determine the Chaboche model parameters, (*YS*, *C,* and *γ*). The test is performed using strain-controlled method. Symmetric strain amplitude is applied. The dimensions of the samples are shown in Figure 8-*a*. In addition, there are holes on the specimen. These holes ensure that cantilever supports are ensured at the ends of the specimen during the tension and especially compression strokes. Figure 8-*b* shows a stable loop obtained at room temperature using a symmetrical strain-controlled loading method. The diagram includes the true stress and true plastic strain where its elastic portion is removed. The deformation ranges are ± 0,08, ±0,06, ±0,03, ±0,05 (strain ratio $R = -1$). The test is conducted at a strain rate of 1 mm/min (0,00033 Hz for a 50-mm gage length). The Shimadzu-Autograph 100 kN tensile testing machine is also utilized to perform this test. The test is performed at room temperature. The experimental data were pre-processed to remove for smoothness in the loop shape.
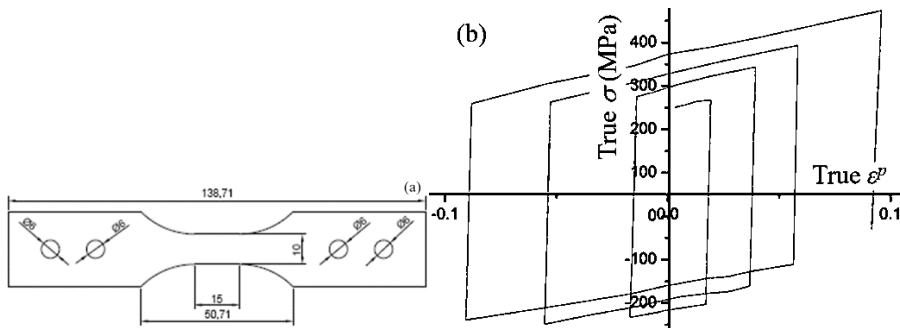
Figure 8. (*a*) Test Specimens (*b*) Low Cycle Fatigue Test Data (3 loops)

The Chaboche hardening rule consists of one term. Table 3 shows the coefficients. Since the deformation is low in the pipe bending process, only the innermost of the 3 loops in the graph is used. Nonlinear regression is performed on this loop data. The "preprocessor→material Props→materials models→structural→nonlinear→inelastic-plastic curve fitting" module in the mechanical APDL module of Ansys© is used for the regression. $\{YS, C, \gamma\}$ are considered as the parameters. Initially, these parameters were set to 1. The maximum number of iterations was limited to 1000 in order to control the computational process. Additionally, normalized error, residual, and coefficient

tolerance were utilized as additional criteria to stop the iterations. In order to achieve the best fit, the goals for these criteria were set to zero. For the error minimization, the Levenberg-Marquard's optimization algorithm was employed. The confidence level for the curves was set at 95%, ensuring a reliable estimation of the results. After the regression, Table 3 shows Chaboche's parameters.

Table 3. Chaboche Parameters

	YS (MPa)	C (MPa)	γ
Values	360	3500	90

4. CONSTITUTIVE EQUATION

Also referred to as the plasticity model, the constitutive equation consists of a yield hypothesis, a hardening rule, and a flow rule. The following section delves into the plasticity model utilized in the study.

4.1. Yield Criteria

General equation of the Von Mises yield function is given in Eq. (1).

$$f(\sigma_{ij}) = \emptyset(\sigma_{1,2,3}) - (\bar{\sigma})^2 = 0 \tag{1a}$$

$$\emptyset(\sigma_{1,2,3}) = \frac{|\sigma_1 - \sigma_2|^2 + |\sigma_2 - \sigma_3|^2 + |\sigma_3 - \sigma_1|^2}{2} \tag{1b}$$

where $\bar{\sigma}$ is the equivalent stress, $\emptyset(\sigma_{1,2,3})$ is its yield function and $\sigma_{1,2,3}$ are principal stresses. Similarly, the Tresca yield function is given in Eq. (2).

$$f(\sigma_{ij}) = \emptyset(\sigma_{1,2,3}) = (\bar{\sigma}) \tag{2a}$$

$$\emptyset(\sigma_{1,2,3}) = max(|\sigma_1 - \sigma_2|, |\sigma_2 - \sigma_3|, |\sigma_3 - \sigma_1|) \tag{2b}$$

4.2. Hardening Rule

Equation (3) is a general yield function which includes both kinematic (α_{ij}) and isotropic (σ_h) hardening rules.

$$\bar{\sigma}(\sigma_{ij} - \alpha_{ij}) - \sigma_h = 0 \tag{3}$$

where, the term α_{ij} is called "back stress" and some α_{ij} functions α_{ij} suggested by Prager, Armstrong-Frederic, Chaboche, Yoshida-Uemori etc… In this study, only Chaboche rule is used. Therefore $\sigma_h = 0$ as seen in Eq. (4). The term α_{ij} which is involved in the equation, indicates that the origin of the surface drawn by the equation will change from center to α_{ij}. Thus, different hardening formations are possible in the tensile and compression zones.

$$\bar{\sigma}(\sigma_{ij} - \alpha_{ij}) = 0 \tag{4}$$

In this study, the back stress equation of Chaboche is used and is given in equation (5).

$$(\dot{\alpha}_{ij})_m = \underbrace{\frac{2}{3} C_m \dot{\varepsilon}_{ij}^{\;p}}_{\text{lineer terim}} - \underbrace{\gamma_m (\alpha_{ij})_m \sqrt{\frac{2}{3} \dot{\varepsilon}_{ij}^{\;p} : \dot{\varepsilon}_{ij}^{\;p}}}_{\text{recall term}} + \underbrace{\frac{1}{C_m} \frac{\partial C_m}{\partial T} (\alpha_{ij})_m \dot{T}}_{\text{Isitma hızı terimi}} \qquad m=1,2,\dots n \tag{5}$$

where, the T temperature, C_m hardening module and γ_m are the coefficients of the reduction of the hardening ratio. These parameters have different values for each term. All of these parameters are determined in the same regression process. The regression process is applied to one hysteresis loop obtained from low cycle fatigue test. Chaboche's back stress equation is a first-order ordinary differential equation. For the single-termed case (first-order), and no change in temperature, Eq. (6) will be achieved when this differential equation is integrated explicitly integrated according to ε_{ij}^p.

$$\alpha = \varphi \frac{c}{\gamma} + \left(\alpha_0 - \varphi \frac{c}{\gamma}\right) e^{-\varphi\gamma(\varepsilon^p - \varepsilon_0^p)} \tag{6}$$

In the equation, α_0 initial back stress value, ε_0^p is the initial plastic deformation value, φ is the sign depending on the tension/compression cases, $\varphi = sgn(\sigma - \alpha) = \pm 1$. In the case of uniaxial tensile, $\varphi = 1 = 1$ and $\varphi = -1$ in case of compression. In uniaxial tensile tests, assume the initial back stress $\alpha_0 = 0$ and the initial plastic deformation $\varepsilon_0^p = 0$. In this case, the back stress equation is given by Eq. (7).

$$\alpha = \frac{c}{\gamma}\left(1 - e^{-\gamma(\varepsilon^p)}\right) \qquad\qquad \text{in tensile stroke } (7a)$$
$$\alpha = \frac{c}{\gamma}\left(-1 + e^{\gamma(\varepsilon^p)}\right) \qquad\qquad \text{in compressive stroke } (7b)$$

The Chaboche equation gives α_{ij}. It is necessary to substitute it in the equivalent stress equation of the yield criterion as $\bar{\sigma}(\sigma_{ij} - \alpha_{ij}) - \sigma_0 = 0$ where σ_0 is the initial yield strength. In the case of uniaxial tensile, since the stress value in the tensile axis is already the principle stress, the equivalent stress in the uniaxial tensile will also be equal to the tension in the main axis x as $\bar{\sigma}(\sigma_{ij} - \alpha_{ij}) = \sigma_x$. In this case, the equivalent stress becomes as follows.

$$\bar{\sigma}(\sigma_x - \alpha_x) = 0 \tag{8a}$$
$$\sigma_x - \alpha_x = 0 \tag{8b}$$

If the expressions in Eq. (7) are moved to Eq. (8), then the stress value will be added to the yield criterion function (Eq. 9).

$$(\sigma_x)_t = \frac{1}{2} + \frac{c}{\gamma}\left(1 - e^{-\gamma(\varepsilon_x^p)}\right) \qquad\qquad \text{in tension } (9a)$$
$$(\sigma_x)_c = -\frac{1}{2} + \frac{c}{\gamma}\left(-1 + e^{\gamma(\varepsilon_x^p)}\right) \qquad\qquad \text{in compression } (9b)$$

4.3. Flow Rule

A flow rule is required to calculate the plastic strain (ε_{ij}^{p}) and its direction. It provides the relationship between plastic deformation and stress. There are two types as associated flow rule and non-associated flow rule. The general equation of a flow rule is $d\varepsilon_{ij}^{p} = d\lambda \frac{\partial f}{\partial \sigma_{ij}}$ and the term λ is called the plastic multiplier. The expression f is a scalar function and is also called the plastic potential. If the yield stress is taken as the potential function, this equation becomes "associated flow rule". Otherwise, it is called non-associated flow rule. The associated flow rule is good at metals, while the non-associated flow rule is good at soil material.

5. CAP DEFORMING SIMULATIONS

Utilizing ANSYS© software, the deformation process is simulated through finite element analysis using an axial symmetric model for convenience, owing to all bodies have cylindrical shape. In the model, the *y*-axis is the axial symmetry axis. The cross-section of the geometry must be in the positive *x*-direction. The friction coefficient of 0,125 is established between the punch, die, and pipe. Punch and die tools are modeled as rigid bodies to shorten the calculation time of the simulation. The pipe is modeled as a flexible body using St52 material and Chaboche's plasticity model. Both bodies are assigned elastic properties from Table 2, while plastic properties from Table 3 are specifically designated for the pipe body. The punch is progressively moved towards the pipe body, as depicted in Figure 9. Initially, a dynamic analysis is conducted to induce plastic deformation in the pipe, followed by an optimization process aimed at calibrating the parameters of Chaboche model.
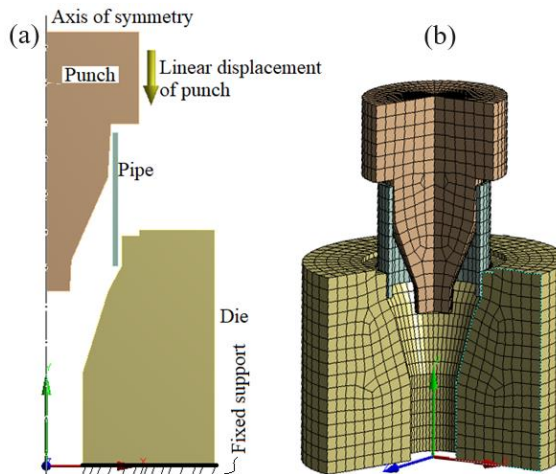
Figure 9. An Axial Symmetric Model of The Cold Forming Process and Its Finite Element Model (*a*) Axial Symmetric Model (*b*) Section View of The Finite Element Model

First, a mesh independence analysis is performed to ascertain the most suitable mesh size (Akkuş and Demir, 2016). The primary focus of this investigation lies in the evaluation of equivalent stress. It is observed that the stress results exhibit minimal variations beyond the utilization of 6845 elements. Consequently, the case with 6845 elements is chosen as the optimal element count. The simulations were executed on a computer equipped with a quad-core processor operating at 3,40 GHz and 8 GB of RAM.

6. OPTIMIZATION

The concept of optimization in mathematics involves the determination of the maximum, minimum, root, or any other value of a given function. In the optimization process, the effects of the Chaboche coefficients (*YS, C, γ*) on the pipes four diameters measured experimentally is determined using various combinations of *YS, C,* and *γ*. The combination providing the best simulation results closest to the experimentally obtained diameter values, will be selected as a candidate point of optimum value. Subsequently, these candidate points undergo verification through analyses.
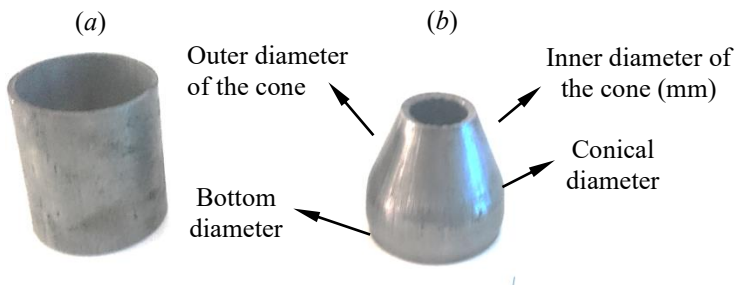
Figure 10. Cold Forming Process of The Pipe (*a*) Before and (*b*) Cold Forming

The experimental measurements are presented in Table 4. Figure 10 shows the cap before and after the deformation. At the beginning, the pipe's outer diameter is 70 mm and thickness is 1,5 mm. The pipe is shown in Figure 10-*a* and *b* before and after cold forming, respectively.

Table 4. Experimental Measurements of The Pipe

Before shrinking		After shrinking		
Inner radius of the pipe (mm)	Outer diameter of the pipe (mm)	Bottom diameter (mm)	Inner radius reduction (mm)	Conical diameter (mm)
Nominal: 21,00	Nominal: 45,00	Nominal:7 3,00	Nominal: 12,50	Nominal: 70,00
21,52	45,44	72,67	12,335	69,85
21,94	45,24	73,03	12,515	70,00
21,75	44,77	73,08	12,540	70,37
21,79	45,20	73,00	12,500	71,09
21,83	45,23	72,95	12,475	69,59
21,78	45,57	72,90	12,450	69,44
21,96	45,21	73,57	12,785	70,12
21,75	45,45	72,79	12,395	69,98
21,81	45,29	72,97	12,485	70,38
21,92	45,45	73,37	12,685	70,40

In this study, for optimization, the constraints and the goals are applied as follows:

- No constraint for *YS*, which is an input variable
- No constraint for *C*, which is an input variable
- No constrain for γ, which is an input variable
- Bottom diameter should be 73 mm, which is an output variable
- Inner radius reduction should be 12,5 mm, which is an output variable

To achieve these aims and constrains, the upper and lower limits of the parameters are determined as in Table 5.

Table 5. Lower and Upper Limits of Design Variables Entered Into The Software

	YS (MPa)	*C* (MPa)	γ
Initial values	360	3500	90
Lower bound	300	2500	10
Upper bound	400	4000	100

7. RESULTS AND DISCUSSIONS

7.1. Response Surface of Optimization

The optimization module calculates the 56 design points (DPs) inside the upper and lower limits. DPs created by the optimization module and the outputs (inner radius reduction, bottom diameter) obtained at the end of the solution for each point are presented in Table 6.

Table 6. DPs and Corresponding Response Points

Number of DPs	Inputs			Outputs	
	YS (MPa)	C_1 (MPa)	γ_1	Inner radius reduction (mm)	Bottom diameter (mm)
1	370,000	3500,000	0,000000	12,1962	73,18609
2	369,9711	3007,191	23,31146	12,1962	73,23054
3	379,8293	3919,364	28,29513	12,19175	73,22193
4	374,3359	3995,884	2,593364	12,19129	73,20807
5	365,3523	3500,196	48,50218	12,19688	73,29505
6	360,0188	3597,085	13,16833	12,19694	73,17549
7	375,5858	3528,72	49,69065	12,19314	73,23783
8	369,9043	3984,597	46,55082	12,19621	73,21676
9	378,6832	3037,863	0,003689	12,19362	73,24799
10	379,8508	3994,644	49,5338	12,19223	73,22158
11	360,5086	3123,173	0,524996	12,1951	73,22787
12	364,6386	3958,324	2,361524	12,19671	73,29525
13	367,9182	3015,39	17,99522	12,19234	73,22602
14	379,8719	3744,171	16,69261	12,19223	73,18767
15	360,2709	3459,992	21,42955	12,19711	73,19113
16	379,1344	3374,817	15,78162	12,15288	73,23748
17	372,1451	3747,933	22,95937	12,19506	73,28925
18	372,3878	3220,819	48,0699	12,19375	73,19387
19	364,8329	3337,762	16,75598	12,19473	73,20053
20	364,6629	3218,356	30,47663	12,19671	73,22603
21	379,2263	3827,115	16,58148	12,17777	73,18016
22	365,1178	3678,777	21,36091	12,19606	73,26566
23	373,4013	3253,686	12,63112	12,19525	73,18251
24	375,741	3991,505	26,64477	12,19304	73,18009
25	366,0642	3000,393	49,55488	12,19675	73,25046
26	369,791	3801,112	4,127309	12,19623	73,18312
27	360,0526	3950,603	16,39369	12,19689	73,69971
28	360,8615	3688,096	44,36721	12,19486	73,2176
29	369,1803	3413,615	27,79114	12,19628	73,18089

30	370,3936	3673,645	49,64961	12,19613	73,22739
31	360,0542	3009,542	45,66033	12,19677	73,23484
32	373,0768	3011,189	5,623021	12,195	73,24051
33	365,2109	3980,406	30,26518	12,1969	73,25545
34	361,0191	3325,248	48,40544	12,19626	73,23605
35	366,8857	3168,001	5,677711	12,19667	73,27455
36	375,6488	3043,843	29,27166	12,19282	73,20419
37	379,8477	3990,551	4,899942	12,19223	73,24825
38	379,3254	3724,445	48,87776	12,19349	73,27701
39	378,7645	3315,722	45,24926	12,1312	73,40294
40	364,7521	3448,275	8,176088	12,1967	73,23751
41	365,8018	3783,93	46,40871	12,19682	73,24381
42	365,3909	3610,448	11,61875	12,19682	73,23469
43	363,2213	3000,526	17,08417	12,19505	73,24944
44	370,6	3981,152	17,16523	12,1961	73,21002
45	375,2963	3875,633	49,06934	12,19313	73,24169
46	373,5455	3519,123	26,83396	12,19524	73,23474
47	369,4801	3299,906	15,08326	12,19602	73,2461
48	379,6503	3048,764	48,05395	12,19231	73,20726
49	360,7634	3996,324	19,5934	12,19487	73,17475
50	379,8577	3127,642	26,50647	12,19223	73,23571
51	376,4269	3692,453	31,80996	12,13284	73,16684
52	367,9349	3315,648	48,59544	12,13438	73,28147
53	360,0196	3189,515	20,8113	12,19678	73,2991
54	379,9752	3554,105	0,61561	12,19173	73,28128
55	379,413	3525,533	37,95053	12,15377	73,19382
56	372,3861	3000,841	43,86515	12,19375	73,18608

It should be noted that these values are the values obtained as a result of simulation. The optimisation module uses them to determine a function based on curve fitting. This function is called response surface. It is shown in Figure 11. Both are created by an artificial neural network with one hidden layer and 3 neurons in. It is a type of multi-layer perceptron.
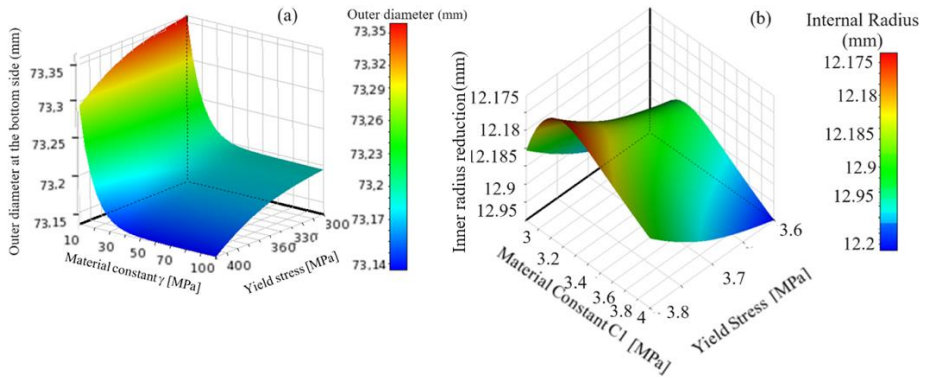
Figure 11. For (*a*) Outer Diameter and (*b*) Inner Radius, Response Surface Diagrams Showing The Relationship Between Input and Output Design Variables in The Optimization

7.2. Optimum Values

The optimum parameters are suggested as given in Table 7. Four optimization methods are employed such as MOGA (Multi-Objective Genetic Algorithm), NLPQL (Nonlinear Programming with Quadratic Lagrangian), MISQP (Mixed Integer Sequential Quadratic Programming), and screening.

Table 7. Candidate Points Suggested by Optimization Methods

Optimization methods	C (MPa)	γ	YS (MPa)	Inner radius reduction (mm)	Bottom diameter (mm)
Screening	3440,9	47,627	375,65	12,49878	73,18470
MOGA	3062,2	43,567	379,73	12,50156	73,16972
NLPQL	3513,7	47,955	370,78	12,50063	73,01945
MISQP	3513,7	47,955	370,78	12,50063	73,01945

The optimization module suggests the candidate points as optima. However, these values are obtained from the response surface by the optimization tool and need to be verified by re-simulating. The verification results are given in Table 8. As seen from table, NLPQL and MISQP provides the best fit where YS=370,73 MPa, C=3513,5 MPa, and γ=47,958.

Table 8. Verified Results

Optimization methods	C (MPa)	γ	YS (MPa)	Inner radius reduction (mm)	Bottom diameter (mm)
Screening	3440,5	47,658	375,676	12,49685	73,18470
MOGA	3062,6	43,556	379,77	12,50685	73,19265
NLPQL	3513,5	47,958	370,73	12,50058	73,01964
MISQP	3513,5	47,958	370,73	12,50058	73,01964

7.3. Stress and Strain Response

As initial values *YS=360 MPa, C=3500 MPa,* and *γ=90* are used, the obtained deformation results are given in Figure 12. Figure 13 gives the total strain and stress responses of the material collected from simulation. Figure 12 also gives Von Mises stress distribution on the deformed cap. The results are captured in the last sub-step of the last step.
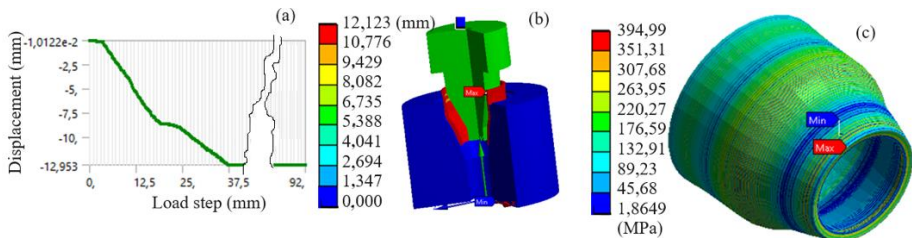
Figure 12. (*a*) Load Steps Applied and (*b*) Total Deformation Results (*c*) Von Mises Stress Distribution When *YS*=360 MPa*, C*=3500 MPa, and *γ*=90
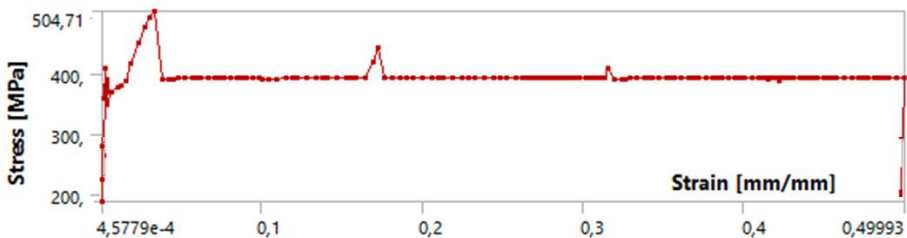
Figure 13. Stress and Total Strain Diagram Obtained From The Analysis

As the optimum values *YS*=370,73 MPa, *C*=3513,5 MPa, and *γ*=47,958 are used, the obtained deformation results (inner diameter reduction) are given in Figure 14. Figure 15 gives Von Mises stress distribution.
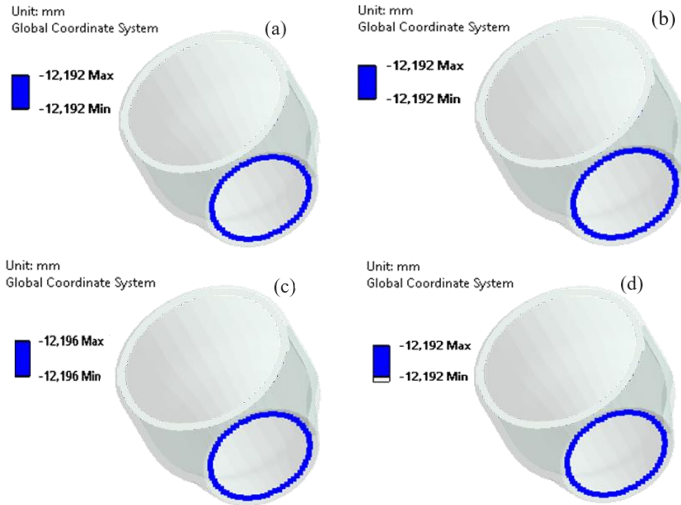
Figure 14. Inner Diameter Reduction (*a*) Screening, (*b*) MOGA, (*c*) NLPQL, (*d*) MISQP
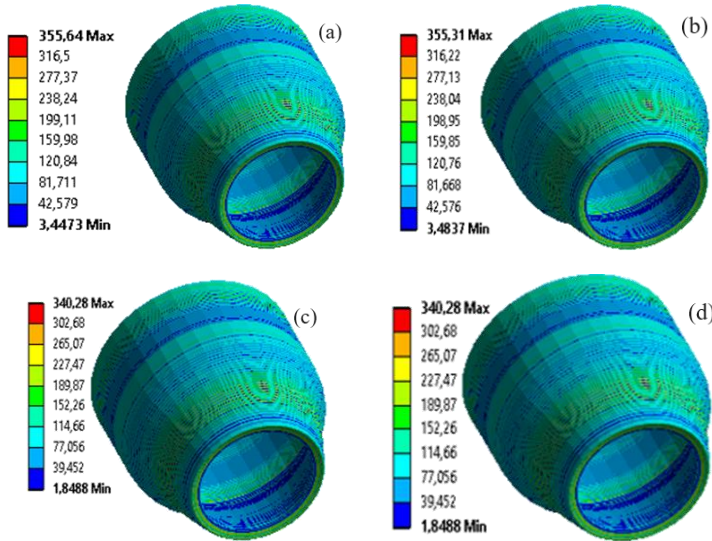
Figure 15. Von Mises Stress Distribution (MPa) (*a*) Screening, (*b*) MOGA, (*c*) NLPQL, (*d*) MISQP

8. CONCLUSIONS

The drag links play a crucial role in the automotive industry. This research employs a finite element simulation to analyse the deformation process of a drag link's cap made from St52 alloy. The plasticity model incorporates Chaboche's nonlinear kinematic

hardening rule, along with the associated flow rule and Von Mises yield criterion. The Chaboche parameters are determined through low cycle fatigue tests, utilizing curve fitting techniques on a single hysteresis loop. Additionally, the Chaboche model parameters are fine-tuned through various optimization techniques. Four optimization methods were performed to calibrate these test data. The main findings obtained from the investigations are listed below:

- The most consistent results are obtained without any dependency on initial values by the NLPQL and MISQP central differences method. Therefore, Chaboche's calibrated parameters are YS=370,73 MPa, C=3513,5 MPa, and γ=47,958.
- Response surfaces are obtained using the neural network method with one hidden layer and 3 neurons.
- The success of optimization methods strongly depends on both the initial values and the lower-upper bounds of the input variables. Any initial value can be selected technically. However, the raw parameters determined after curve-fitting can be used as initials. Their bounds should be set as half and two-times below and above their initial values, respectively.
- This study has future work potentials to investigate the combined hardening rules with more terms.

Author Contributions
All authors contributed equally.

Conflicts of interest
The authors declare that they have no conflicts of interest or competing interests regarding the publication of this paper.

Data and Code Availability
The data used in the study have already been given in the figures or tables.

Research and Publication Ethics Statement
Research and publication ethics were followed in the study.

REFERENCES

Akkuş, Ö. & Demir, E. (2016). İki düzeyli olasılık modellerinde klasik meta sezgisel optimizasyon tekniklerinin performansı üzerine bir çalışma. *Istanbul Commerce University Journal of Science*, 15(30), 107-131.

Armstrong, P.J. & C.O. Frederick, (1966). A mathematical representation of the multiaxial Bauschinger effect. *CEGB Report*, RD/B/N731, Berkeley Nuclear Laboratories.

Chaboche, J.L., (1986). Time-independent constitutive theories for cyclic plasticity. *International Journal of Plasticity*, 2(2);149-188.

Chaboche, J.L., (1989). Constitutive-equations for cyclic plasticity and cyclic viscoplasticity. *International Journal of Plasticity*, 5(3): p. 247-302.

Cruise R.B. and Gardner L. (2008). Strength enhancements induced during cold forming of stainless steel sections. *Journal of Constructional Steel Research*, 64(11), 1310-1316.

Ditas Corp., (2019). Drag link, Retrieved January 07, 2019 from http://www.ditas.com.tr/drag-link

Kacar, İ. (2023). Scientific Principles of Mechanical Design and Analysis. *Akademisyen Puplishing House*, Ankara, First ed., 36-40.

Kuhn, H. A. Lee P.W. & Erturk T. (1973) A fracture criterion for cold forming. *Journal of Engineering Materials and Technology*, 95(4): 213-218.

Prager W., (1949). Recent developments in the mathematical theory of plasticity. *Journal of Applied Physics*, 20(3): 235-241.

Sevenler K., Raghupathi P.S., & Altan T., (1987). Forming-sequence design for multistage cold forging, Journal of Mechanical Working Technology, 14 (2), 121-135.

Ziegler, H., (1959). A modification of Prager's hardening rule. *Quarterly of Applied Mathematics*. 17(1): 55-66.